sustainability

MDPI

Article

A Study of Sandy Land Changes in the Chifeng Region from 1990 to 2020 Based on Dynamic Convolution

Hongbo Zhu [1], Bing Zhang [1,2,*], Xinyue Chang [1], Weidong Song [1,2], Jiguang Dai [1,2] and Jia Li [3]

[1] School of Geomatics, Liaoning Technical University, Fuxin 123000, China; 47211053@stu.lntu.edu.cn (H.Z.); 472120793@stu.lntu.edu.cn (X.C.); songweidong@lntu.edu.cn (W.S.); daijiguang@lntu.edu.cn (J.D.)
[2] Collaborative Innovation Institute of Geospatial Information Service, Liaoning Technical University, Fuxin 123000, China
[3] Dalian Huangbohai Marine Surveying Data Information Co., Ltd., Dalian 116000, China; simplaghy@163.com
* Correspondence: zhangbing@lntu.edu.cn

Abstract: Desertification is the process of land degradation and the reduction or destruction of biological potential in arid, semi-arid, and semi-humid areas, and its impact on agricultural development and the ecological environment cannot be ignored. Therefore, many researchers have aimed to achieve the acquisition of large-scale sandy land areas using sandy land extraction algorithms based on remote sensing images. However, the sandy land extraction accuracy needs to be improved because of the variable contour features in the remote sensing images and the easy confusion with targets such as the Gobi and bare ground areas. In this study, we combine the dynamic convolution with a U-Net model and propose the DU-Net sandy land extraction model. The method is based on dynamic convolution, which can adaptively learn the complex features of the target and build a dynamic convolutional neural network to achieve high-accuracy extraction of complex targets. DU-Net achieved 86.32% in IoU, 93.22% in precision, 94.5% in recall, and 92.66% in F_1-score in sandy land extraction accuracy, which are 4.68%, 2.33%, 3.09%, and 2.76% improvements, respectively, compared with the U-Net static neural network. Based on this, we obtained the spatial and temporal evolution trends of sandy land areas based on Landsat images in the Chifeng region in the Inner Mongolia Autonomous Region, China. Meanwhile, in order to investigate the mechanism of spatial and temporal changes in the sandy land area in the study region over the past 30 years, the direct and indirect effects of seven climatic and human socioeconomic activity factors on the changes in the sandy land area in the study region were evaluated based on a structural equation model. The results show that the sandy area in the Chifeng region tended to first increase and then decrease over the study period, with the sandy land area reaching its maximum around the year 2000. In addition, the main driving factor for the change in the sandy land area in the Chifeng region has been human socioeconomic activities, with climatic conditions as the secondary driving factor. The method proposed in this paper realizes the rapid extraction of sandy land areas with high accuracy at a large scale and with a long time series and provides a basis for assessing the effectiveness of ecosystem restoration projects.

Keywords: dynamic convolution; changes in sandy land area; structural equation model; driving force analysis; U-Net

check for updates

Citation: Zhu, H.; Zhang, B.; Chang, X.; Song, W.; Dai, J.; Li, J. A Study of Sandy Land Changes in the Chifeng Region from 1990 to 2020 Based on Dynamic Convolution. *Sustainability* **2023**, *15*, 12931. https://doi.org/10.3390/su151712931

Academic Editor: Matteo Gentilucci

Received: 14 July 2023
Revised: 22 August 2023
Accepted: 25 August 2023
Published: 27 August 2023

Copyright: © 2023 by the authors. Licensee MDPI, Basel, Switzerland. This article is an open access article distributed under the terms and conditions of the Creative Commons Attribution (CC BY) license (https://creativecommons.org/licenses/by/4.0/).

1. Introduction

Desertification refers to the degradation or destruction of bio-potential in arid, semi-arid, and semi-humid regions, which has a great influence on both agriculture and the eco-environment [1–3]. It destroys land resources, reducing the area of land available for agriculture and grazing, degrading the fertility of the land, reducing the amount of vegetation, and decreasing the carrying capacity of the land and the yield of crops. Because of the wide spatial and temporal distribution and the heterogeneity of desertification, the

method of determining desertification indicators using visual interpretation of remote sensing data can be used to obtain its spatial and temporal distribution. However, this is not an effective approach because it is difficult to satisfy the requirements of the large scale and long duration of desertification monitoring with this approach [4,5].

The study of desertification extraction and monitoring has become more intense as remote sensing technology has advanced. Desertification extraction approaches based on remote sensing images can be classified as computer graphics-based threshold segmentation methods, spectral index extraction methods, and machine learning classification extraction methods. Among the different methods, the extraction of desertification based on threshold segmentation [6–8] can determine the classification sample category and control the sample classification threshold in advance, based on expert experience. However, the extraction accuracy is relatively low and the universality is not high because threshold segmentation is a simple approach, for which it is difficult to determine the segmentation threshold, and the spectral features of sandy land areas are typically complex. Although the spectral index extraction methods can use spectral information to improve the extraction accuracy, compared to the classifier-based methods, this type of method has the problem of complicated construction of the spectral index [9,10]. Deep learning-based techniques have been widely explored in the field of computer vision in recent years, as a significant branch in the science of machine learning [11,12].

Convolutional neural networks (CNNs) are the most well-known and widely used deep learning algorithms [13], with the characteristics of local connectivity and weight sharing, which can reduce the network complexity, reduce the number of parameters, and perform much better than the traditional machine learning algorithms. As a result, CNNs are now widely used in image processing [14]. On this basis, Long et al. [15] proposed the fully convolutional network (FCN), which replaces the fully connected layer in a CNN with a convolution operation to reduce the class of each image element from the extracted features. As a result, remote sensing image classification can be extended from the image level to the pixel level, preserving the high-resolution spatial information of the imagery, reducing the model parameters, and improving the efficiency of the algorithm. The U-Net model proposed by Ronneberger et al. [16] consists of an encoding path that captures the contextual information and a decoding path for precise localization, which improves the model performance by stitching high-resolution features with the decoder upsampling output features using a skip connection structure. Because of its benefits of high extraction accuracy, compact model operations, and high model accuracy, even with a limited number of samples, U-Net is increasingly commonly utilized in the field of remote sensing feature interpretation [17–19].

Due to the variable contour features of sandy land areas in remote sensing images and the easy confusion with targets such as Gobi and bare land, the deep learning-based target extraction methods using the target contour as the main feature still have a lot of room for accuracy improvement in the long time series and sandy land extraction tasks. Furthermore, the classic static neural network is trained using a large quantity of data, yielding only a static network model with set parameters, which can only employ fixed model parameters in the model inference and cannot effectively handle many types of input images [20,21]. If a typical static inference model is used in the desertification monitoring task, the model would be disturbed by the complex sandy land characteristics, and the extraction accuracy would suffer as a result of the multi-scale, multi-type, and complicated sandy land characteristics. Dynamic convolution can generate an attention weight matrix based on the variable sanded land features in the image. Then, to generate the final convolution kernel, the attention weight matrix is dynamically aggregated with the matching convolution kernel weights. The proposed dynamic convolution-based model enables accurate extraction of multi-scale complex scenes and irregular targets. In addition, its adaptive establishment of the mapping relationships matching the current input samples by adjusting the convolution kernel parameters and other methods in the model training

stage for multiple types of training samples with different feature distributions can greatly improve the sandy land extraction model's characterization ability [22–24].

As a result, the primary contribution of this study was the development of a sandy land area dynamic extraction model (DU-Net) that combines dynamic convolution with U-Net. To begin with, we improved the characterization ability of the deep learning model for sandy land extraction, based on the previous reports, to achieve fast and accurate extraction of long time series sandy land information in the study region using a combination of dynamic convolution and the classical U-Net target extraction model. The geographical and temporal evolution patterns of the sandy land areas in the research area were then examined from 1990 to 2020. Finally, a structural equation model (SEM) was used to investigate the driving factors of sandy land area changes in the research region. The goals of this research were as follows: (1) in view of the characteristics of the variable contour features of sandy land in remote sensing images and the easy confusion with targets such as Gobi and bare land, a sandy land dynamic extraction model (DU-Net) combining dynamic convolution and U-Net is proposed to achieve the accurate extraction of sandy land with small sample datasets; (2) to investigate the geographical and temporal evolution patterns of sandy land areas in the research region from 1990 to 2020; and (3) to assess the influence of the various natural and human activity factors on sandy land area change.

The remainder of this work is structured as follows. Section 2 explains the research topic and data collection for this work. Section 3 details the dynamic convolution process and SEM theory, as well as the construction technique and SEM for the sandy land dynamic extraction model (DU-Net) that combines dynamic convolution and U-Net. The outcomes of the experiments are provided in Section 4. Section 5 discusses the multi-year spatial and temporal evolution trends of the sandy land areas in the study region, and also describes the set of experiments based on the SEM for assessing the effects of driving factors, such as human activities and climatic conditions, on the changes in the sandy land area in the study region. The limitations of the study and potential future work are also described. Section 6 summarizes and concludes the current work.

2. Study Region and Data

2.1. Overview of the Study Region

The Chifeng region (41°17′–45°24′ N, 116°21′–120°58′ E) is in the eastern part of China's Inner Mongolia Autonomous Region, at the western end of Northeast China, the upper reaches of the Xiliao River, the southwest section of the Daxinganling Mountains, the Inner Mongolia Plateau, and the Xiliao River Plain [25]. The Xilamulun and Laohar rivers run through the heart of the Chifeng region. The Chifeng region has a moderate continental monsoon climate with a lot of rain in the summer and autumn [26]. Because the climate is dry and windy in winter and spring, the spatial and temporal fluctuations of the sandy land areas in this region are vital for production and life, as well as the evolution of ecological patterns.

2.2. Research Information

Landsat 4–5 Thematic Mapper (TM), Landsat 7 Enhanced Thematic Mapper Plus (ETM+), and Landsat 8 Operational Land Imager (OLI) images of seven time phases were employed as the data sources to analyze the geographical and temporal patterns of sandy land areas in the research region from 1990 to 2020, at 5 year intervals. The satellite remote sensing images had a spatial resolution of 30 m, and the data were all remote sensing data with less than 10% cloud cover throughout the vegetation growing season (May–September). The data had already been pre-processed with radiometric calibration, geometric correction, and atmospheric correction [27,28]. The pre-processing conducted in this study included radiometric calibration, geometric correction, and atmospheric adjustment. We used a mixture of bands that are spectrally sensitive to sandy land to synthesize false-color images for the sandy land extraction research, in order to highlight the sandy land characteristics in the images [29]. At the same time, meteorological data (precipitation, evaporation, and

sandy wind days) and yearbook data (population size, livestock volume, arable land area, and ecosystem restoration project area) were also gathered.

3. Research Methodology

3.1. Dynamic Convolution

The proposed DU-Net model integrates dynamic convolution into the U-Net model to boost the expressive capability of the standard CNN. As a result, the DU-Net model can dynamically aggregate sub-networks to build the convolution kernel weights adaptively, depending on the attention weights. AvgPooling is the average pooling layer, while FC is the fully connected layer, as shown in Figure 1. The dynamic convolution module first feeds the input sandy land feature map into the average pooling layer and then feeds it into the softmax layer after fusing the fully connected layer structure with the rectified linear unit (ReLU) activation function to obtain a $1 \times k$ attention weight matrix. Finally, to generate the final convolution kernel, the attention weight matrix is dynamically aggregated with the matching k convolution kernel weights. After generating the dynamic convolution kernel based on the attention weight matrix, the dynamic convolution module inputs the convolved target features to the next process of the DU-Net network, as shown by the arrow on the right side of the Conv block in Figure 1. This approach is capable of dynamically modifying the convolution kernel to the provided diverse samples, in order to adapt to the sample variety by adding just a minimal number of model operations while maintaining the network depth and feature map width. Dynamic convolution can create appropriate convolution kernels adaptively for sandy land targets with multi-scale characteristics in remote sensing images, boosting the model's flexibility for complex and changeable sandy land features. The process of dynamic convolution can be denoted as shown in Equation (1):

$$Y = Conv(x), \sum_{i-1}^{k} Attention_K(x) W_k \quad (1)$$

where x is the module input feature, $Attention_K(x)$ is the attention weight, W_k is the convolution kernel parameter generated by the module adaptively based on the sandy land target features, * as a product relationship, and Conv is the convolution operation.

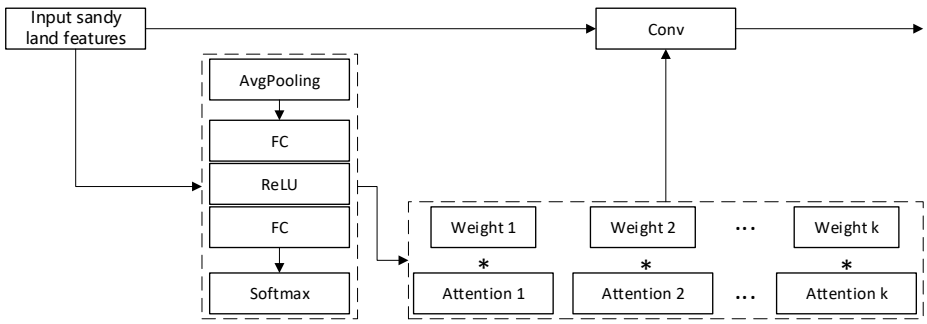


Figure 1. Dynamic convolution module structure diagram.

3.2. DU-Net Sandy Land Extraction Model

The target extraction models based on a deep convolution neural network (DCNN) can achieve high-precision and rapid extraction of sandy land information from remote sensing images through the feature extraction network and upsampling network parts. The encoder part of the sandy land extraction model (DU-Net) proposed in this paper selects the VGG network model based on U-Net, which makes the U-Net model easy to train, reduces the model parameters, and improves the accuracy of the sandy land feature extraction. As shown in Figure 2, in the decoder part, the classical U-Net target extraction model is selected [16]. However, the basic static CNN fails to satisfy the criterion of high-accuracy extraction of sandy land area with a small number of samples, due to the characteristics of sandy land, i.e., the varied sizes, types, and difficult scenarios. Based on the VGG network

model in the encoder part of the model, a dynamic convolution module (D Conv) [29] is introduced into the encoder part instead of the standard 3 × 3 convolution to obtain the dynamic DU-Net model that is suitable for sandy land extraction from remote sensing images. This dynamic CNN structure improves the problem of generalizability needing to be improved due to the inconspicuous target features, diversity, and fixed parameters of the static network. This dynamic convolutional neural network structure improves the problem that the pervasiveness needs to be improved due to inconspicuous target features, diverse representations, and fixed static network parameters. Furthermore, compared to U-Net, the DU-Net model with the dynamic convolution module is easier to train and produces a higher extraction accuracy, even with fewer training samples. In addition, a batch normalization (BN) module is used in the model's decoder to maintain the same distribution of inputs in each layer during the training phase. This enables the model to employ the same size feature map stitching as the downsampling in the upsampling convolution (UP Conv), resulting in improved model reconstruction via the skip connection.

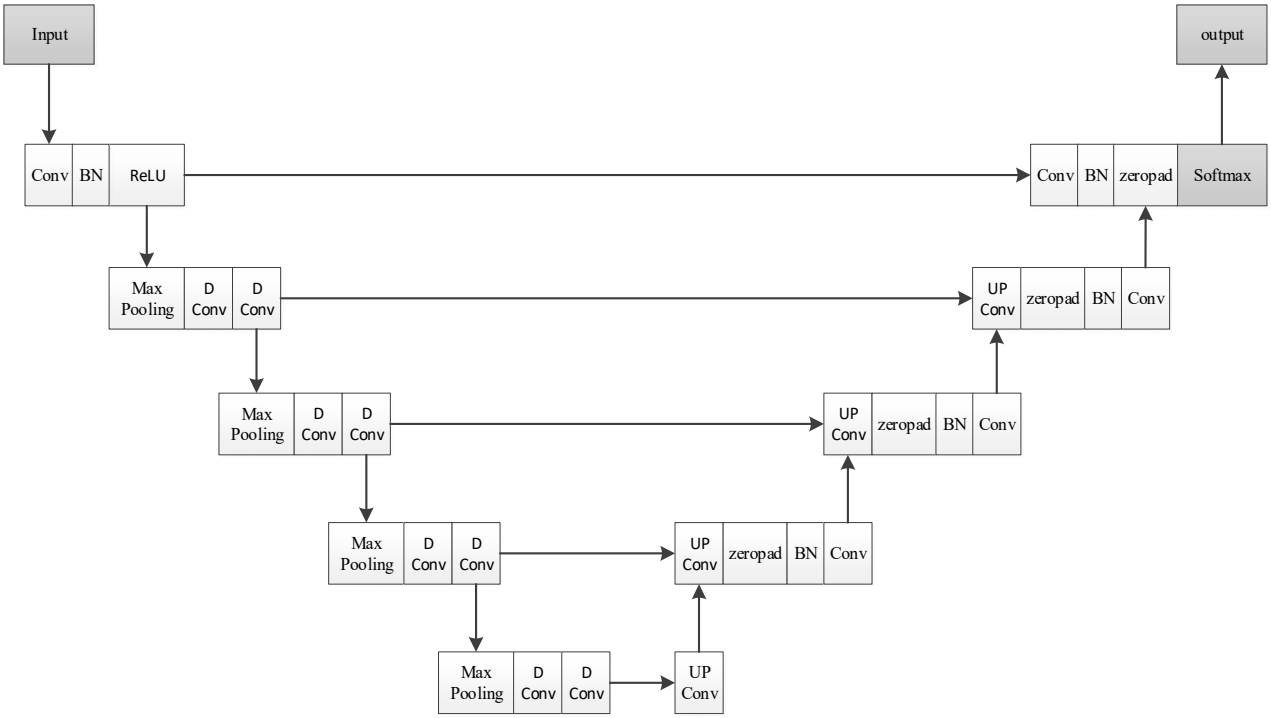


Figure 2. Schematic diagram of the DU-Net model structure.

3.3. Structural Equation Model (SEM)

The SEM is a multivariate statistical tool for explaining the causal link between variables [30]. Compared with traditional multivariate statistical methods, structural equation modeling allows for the measurement of variables with errors and constructs path diagram models based on expert experience. This provides us with the possibility to analyze the relationship between different variables, which has resulted in the SEM being widely used in ecological and environmental fields [31,32]. It is important to consider the coupling of driving factors on the change in the sandy land area, in addition to the direct influence of driving factors such as population size, arable land area, livestock volume, ecosystem restoration project area, precipitation, evapotranspiration, and the number of sandy wind days. Structural equation modeling can analyze both the measurement errors and the structural relationships between potential variables and is not limited by the strict assumptions of path analysis, which can compensate for the difficulty of characterizing the complex coupling relationships between variables. Its central idea is to estimate all the parameters in the model simultaneously using the method of great likelihood estimation and to assess the overall degree of model fit based on the difference between the theoretical model covariance

and the actual measurement covariance. The SEM calculates the covariance matrix between the human socioeconomic activities, meteorological conditions, and long time series sandy land area change to obtain the path coefficients of the path diagram model, and can then quantitatively characterize the effect of multiple driving factors on sandy land area change. The variables in the SEM can be classified into two types: (1) observable variables, which can be immediately observed and measured; and (2) latent variables, which cannot be directly observed and defined. The potential driving factors influencing sandy land area change can be immediately seen and defined, so that the SEM constructed in this study uses only the observed variables as model inputs to investigate the interaction between the seven factors mentioned above and the sandy land area.

3.4. Multivariate Weighted Results

The accuracy of the proposed DU-Net approach in sandy land area extraction with remote sensing images was assessed by constructing a deep learning-based performance evaluation algorithm, in order to obtain an objective assessment of the dynamic sandy land extraction. To begin with, we binarized the sandy land extraction results obtained by the DU-Net sandy land extraction model with the sandy land sample labels accurately labeled by experts, in order to maximize the distinction between sandy land and background in each image, and used the pixel-level comparison results of the two as evaluation indices. Four performance indicators were utilized in this research to assess the proposed approach [33]: Precision, recall, IoU, and F_1-score, which are all specified in Equations (2)–(5). The intersection-to-merge ratio (IoU) is the ratio of the intersection and merging of the extraction results from the same image and the sample label pixels. The greater the value of the index, the greater the agreement between the retrieved findings and the sample labels in the test set.

Precision refers to the number of sandy land pixels extracted by the model that contains the same sandy land pixels as the sample labels. The recall rate refers to the number of pixel points correctly extracted as sandy land by the model. The F_1-score value can balance the effects of precision and recall and evaluate the sandy land extraction model more comprehensively.

$$Precision = \frac{TP}{TP + FP} \tag{2}$$

$$Recall = \frac{TP}{TP + FN} \tag{3}$$

$$IoU = \frac{TP}{TP + FP + FN} \tag{4}$$

$$F_1 = 2 \times \frac{Precision \times Recall}{Precision + Recall} \tag{5}$$

where TP is the number of pixel points in the remote sensing image that are correctly extracted as sandy land by the model; FP is the number of pixels in the image where the other targets that are easily confused with sandy land are mistakenly extracted as sandy land by the model; and FN is the number of pixels in the image where sandy land is misclassified as background, i.e., the number of sandy land pixels missed by the model.

4. Experiments and Analysis

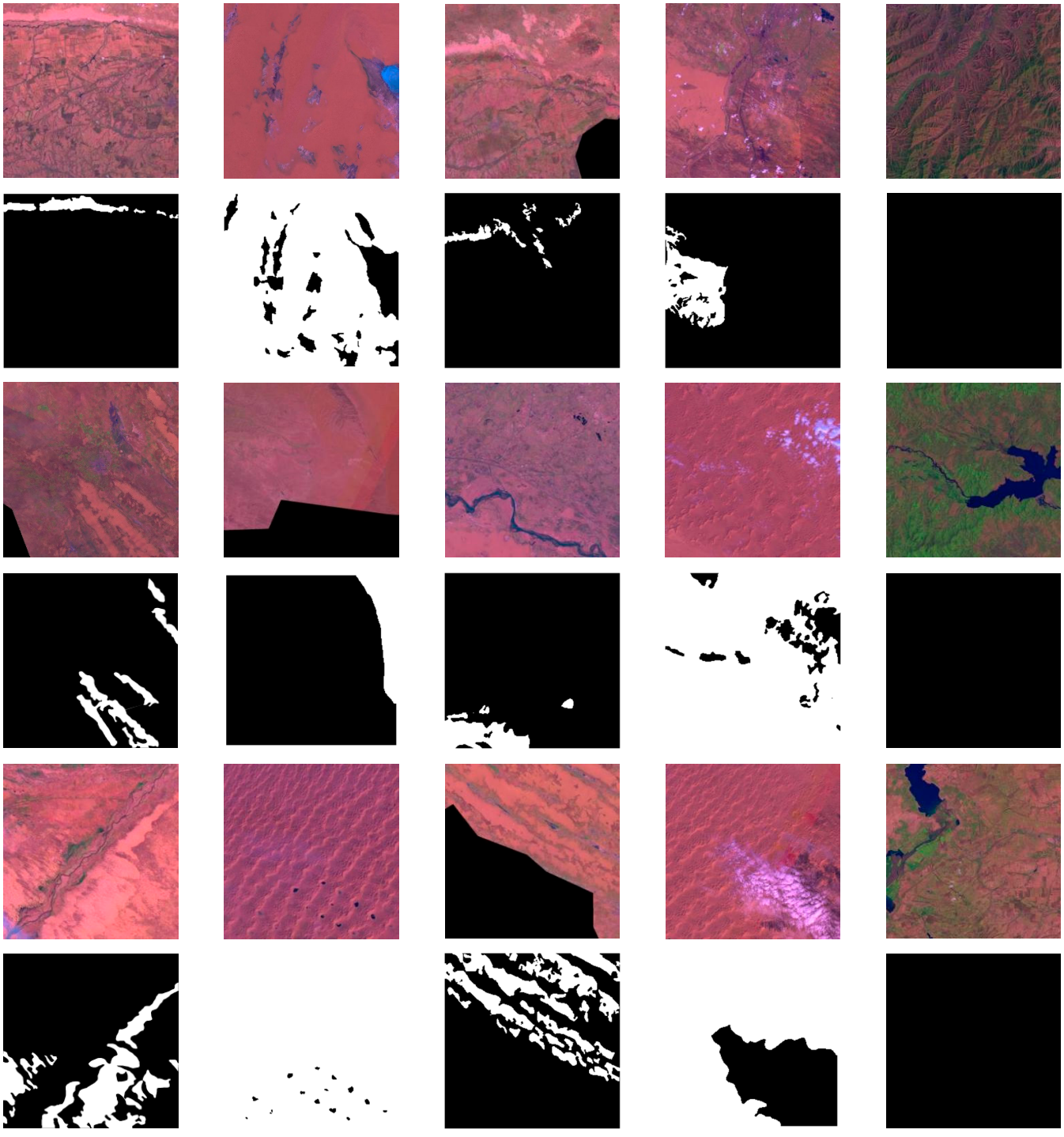
4.1. Experimental Data

In this study, we constructed a benchmark dataset for sandy land extraction using massive Landsat multispectral images from over a large area and multiple years in northern China.

(1) Due to the mobility and spatial heterogeneity of the area and distribution of sandy land areas, they have the characteristics of variable contour features, and the differences in light intensity, cloud coverage, and image background complexity also make the sandy land areas have multi-scale and multi-type characteristics in remote sensing images. To improve

the robustness of the DU-Net sandy land extraction model for sandy land extraction from Landsat multispectral images of different regions, times, and imaging conditions, we acquired Landsat images of different times, regions, and environments in northern China, including the Inner Mongolia Autonomous Region, the Ningxia Hui Autonomous Region, and some regions of Liaoning province, to create a benchmark sandy land extraction dataset. Table 1 shows some examples from the sandy land extraction dataset.

Table 1. Sand extraction datasets in different states.

Normal Image	Low-Brightness Image	Complex Background Image	Cloud Amount Interference Image	Negative Sample
				

(2) The original size of the Landsat multispectral images was large, so we cropped the images with the neighborhood centered on the sandy land area in the image and adjusted the cropped image to 512 × 512 pixels by bilinear interpolation resampling. The dataset was built using varied backdrop complexity, picture brightness, and cloud coverage. A total of 8780 samples were created, including 4780 positive samples and 4000 negative samples that did not have sandy land labels. The dataset was separated into training samples, validation samples, and test samples at an 8:1:1 ratio.

(3) To create label sets, the contour lines of the sandy land areas in the photos were manually tagged using the LabelMe data labeling program. A benchmark dataset for sandy land extraction for deep learning was then created by combining the sample set and its related label set.

4.2. Model Training

The aforementioned training set was utilized in this research to train the sandy land extraction model (DU-Net), for which the training duration was 12.2 h. In Table 2, the "epochs" represent the number of iterations of all the training samples in the training set; the "batch_size" is the number of samples learned by the model in the same iteration; and "train loss" and "val loss" represent the difference between the prediction results and the sample labels in the training and validation sets, respectively. This is quantified by the loss function, i.e., the loss value of the model in the training and validation sets. The learning rate is a parameter for adjusting the degree of fit in the algorithm, which determines the step size in each iteration. The model reached the optimal parameter setting at the 160th epoch.

Table 2. Optimal parameters for model training.

Parameter Indicators	Epochs	Batch_Size	Train Loss	Val Loss	Learning Rate
Parameters	200	4	0.022	0.028	1×10^{-5}

4.3. Experimental Results

Based on 680 test samples made up of precisely labeled sandy land areas from the sandy land extraction benchmark dataset, we investigated the robustness of the proposed technique for sandy land extraction under an extended time series, multiple scales, and natural circumstances. The original U-Net model and the proposed DU-Net model were used to extract sandy land areas from the test set images. The sample labels accurately labeled by the same image experts were used as the true values, and the mean values of the four performance evaluation indices corresponding to the different methods were obtained (Table 3).

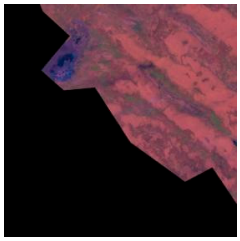
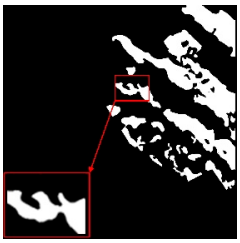
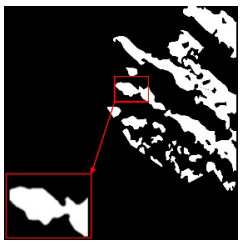
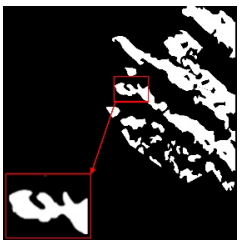
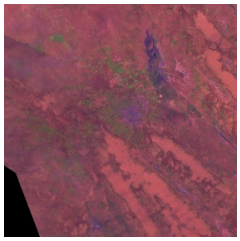
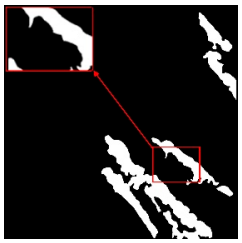
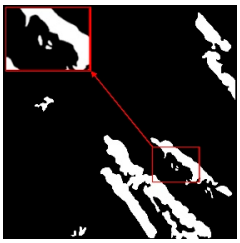
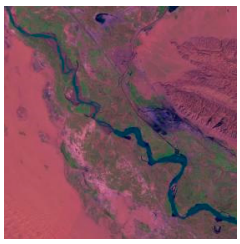
Table 3. Comparison of the sandy land extraction results from Landsat images.

Model	IoU/%	Precision/%	Recall/%	F_1/%
U-Net	81.649	90.890	91.409	89.898
DU-Net	86.324	93.224	94.501	92.660

As shown in Table 3, the results of the sandy land extraction experiments between DU-Net and the classical U-Net model for the test set of the 680 Landsat images containing sandy land show that the fused dynamic convolutional sandy land extraction model (DU-Net) proposed in this paper outperforms the classical U-Net model in all four extraction accuracy performance indices, namely, IoU, precision, recall, and F_1-score. Table 4 also displays the sandy land extraction results for the Landsat images in the test set, using the two approaches described above. In terms of extraction accuracy in the situation of a simple backdrop of remote sensing imagery, the traditional U-Net model is equivalent to the model proposed in this paper. However, the conventional U-Net model can rarely satisfy the

correct extraction of sandy land at different scales in complex scene images, due to the features of no evident texture and irregular form, and the uneven demarcation of sandy land, which leads to the problem of inaccurate sandy land extraction. In this study, dynamic convolution was used to produce the convolution kernel parameters adaptively, based on the characteristics of the sandy land images, resulting in extremely robust extraction of multi-scale sandy land features, which is an approach that is more suited for actual application scenarios.

Table 4. Comparison of the Landsat image sandy land extraction results.

Original Image	True Value Label	U-Net	DU-Net
			
			
			

5. Discussion

Based on the findings of this study, we acquired the geographical and temporal changes in the sandy land areas in the study region from 1990 to 2020. In Section 5.1, we discuss and evaluate the multi-year spatial and temporal patterns in the sandy land areas in the study region. In Section 5.2, we describe the series of experiments based on the SEM conducted to examine the impacts of driving factors such as human activities and meteorological conditions on sandy land area change in the study region. Finally, Section 5.3 discusses the study's weaknesses and possible future research directions.

5.1. Analysis of the Spatial and Temporal Trends of the Sandy Land Areas in the Study Region

Figure 3 depicts the geographical and temporal evolution patterns of sandy land areas in the research region from 1990 to 2020 obtained using the U-Net model with fused dynamic convolution (i.e., the DU-Net model) at 5 year intervals. As shown in Figure 3, the sandy land area in the study region increased and then decreased over the previous 30 years, with the sandy land area reaching its peak around the year 2000, as indicated in Figure 3c. Sandy land areas began to emerge in the northeastern portion of the study region between 1995 and 2000, reaching a maximum area around 2000, as shown in Figure 3c,d. It is worth noting that the geographical distribution of the sandy land areas in the study region is more concentrated in the east and less concentrated in the west, and the area of

sandy land areas in the study region's west decreased constantly between 1990 and 2020, as shown in Figure 3a–c. The area of sandy land areas in the west of the region was negligible around 2005, as shown in Figure 3d, due to the series of ecological restoration measures represented by afforestation and pasture restoration where the sandy areas in the western part of the study region were located. The studies of Zhang et al. [34] and Zhang [35] show that the eastern part of Inner Mongolia, where the Chifeng region is located, has seen an increase in the area of sandy land due to the degradation of pastures. The regional and temporal evolution patterns of the sandy land in the Chifeng region, as determined in this work, are further described by Zhang et al. and Zhang.

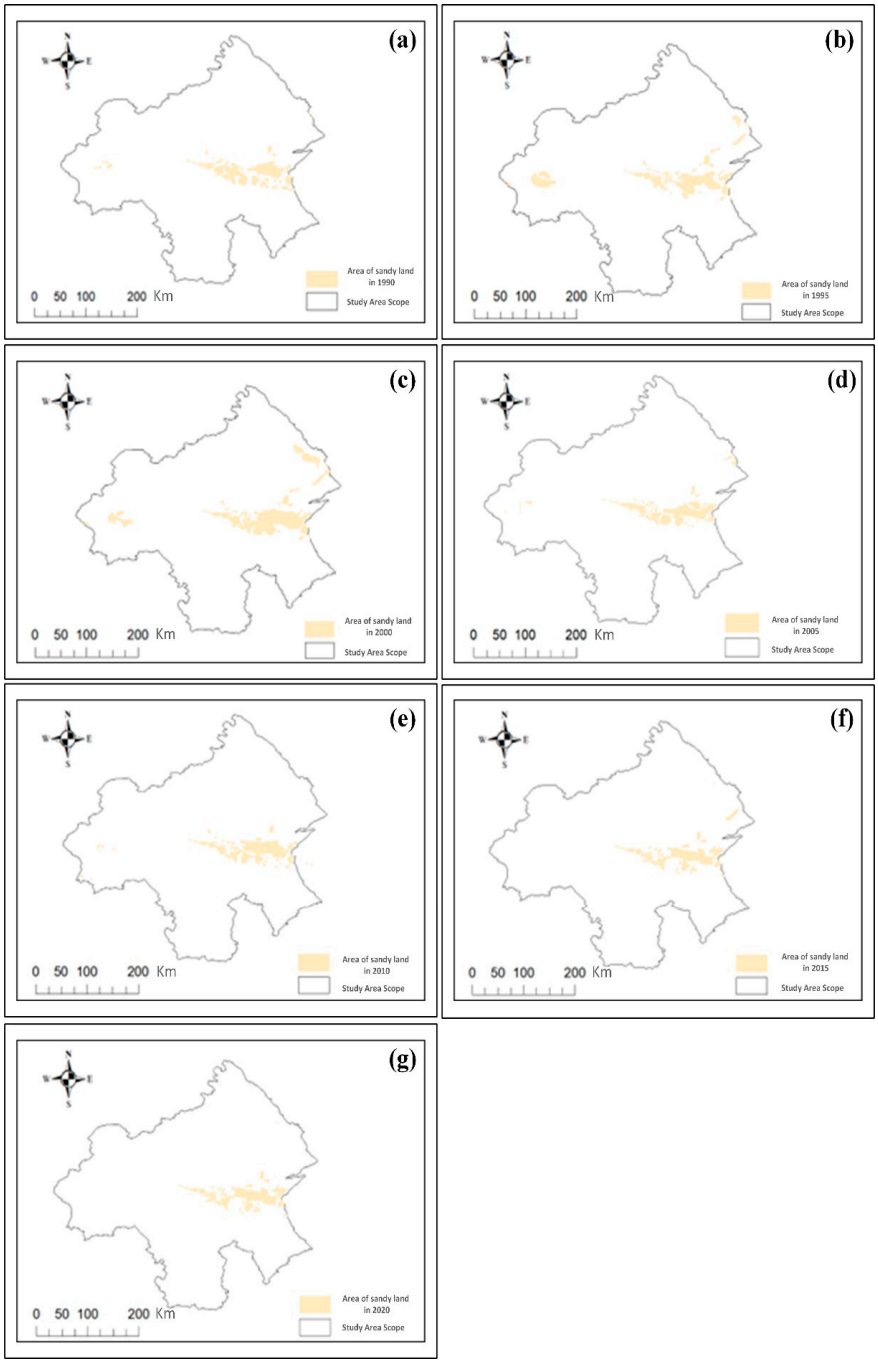


Figure 3. Spatial and temporal distribution of the sandy land areas in the Chifeng region from 1990 to 2020. Note: (**a**–**g**) show the distribution of sandy land areas in the Chifeng region in 1990, 1995, 2000, 2005, 2010, 2015, and 2020, respectively.

5.2. Analysis of the Driving Factors of Sandy Land Area Change from the Structural Equation Modeling Perspective

Since the change in the sandy land area is influenced by a variety of factors coupled with climatic conditions and human socioeconomic activities, in order to investigate the intrinsic driving mechanism of sandy land area change in the Chifeng region during the study period, we constructed an SEM based on seven driving factors, i.e., population size, livestock volume, arable land area, ecosystem restoration project area, precipitation, evaporation, and the number of sandy wind days, using counties and districts as the study units. The SEM path diagram is shown in Figure 4. The observed variables are represented by the rectangular boxes in the path diagram, and two variables connected by a solid line with a single arrow indicate the presence of a causal relationship between variables. A total of 60 samples were utilized to fit the model, and the fitted model's *p*-value was 0.347. It is also crucial to note that the *p*-value range for the SEM differs from the *p*-value range for the data processing task, with a valid interval of 0.05 p1, and the bigger the difference, the better the model fit. The model calculates the SEM parameters using the partial least squares technique (PLS), and all the route coefficients are displayed in the figure. The numbers next to the arrows in the figure are path coefficients, which indicate the degree of causality between two variables. For example, the path coefficient between "Number of Sandy wind days from year" and "Sandy land area" is 0.16, indicating that the direct effect of "Number of Sandy wind days from year" on "Sandy land area" is 0.16. The indirect path between "Ecosystem restoration project area" and "Sandy land area" is calculated as $-0.247 \times 0.16 = -0.039$. The combined path coefficient between the two variables is the sum of their direct and indirect paths [36]. The evapotranspiration and ecosystem restoration project areas exhibit large path coefficients, indicating that they have the biggest effect on sandy land area change in the research region. Table 5 lists the results of calculating the integrated route coefficients between each driving factor and the sandy land area based on the direct and indirect pathways between that component and the sandy land area. The ecosystem restoration project area, evapotranspiration, and the number of sandy wind days are the key factors impacting the change in sandy land area, according to the integrated path coefficients.

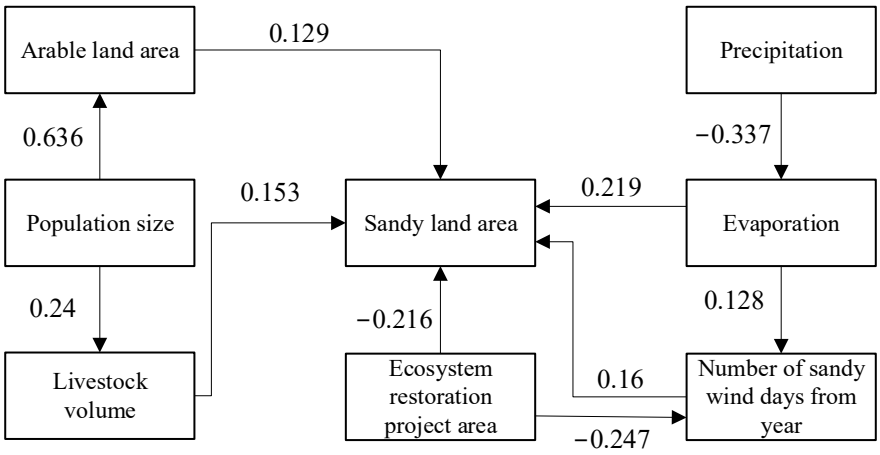


Figure 4. Structural equation model path diagram.

The impact of socioeconomic activities and climatic circumstances on the change in the sandy land area in the study region was estimated individually using the SEM. With the proliferation of arable land between 1990 and 2000, a large number of pastures were destroyed, resulting in a weakening of the sand fixation capacity, which in turn led to the expansion of sandy land in the study region. After 2000, with the introduction of the relevant sand prevention and control policies, ecosystem restoration projects represented by artificial afforestation, grass planting, and integrated management of the small watersheds in the study region were implemented. At the same time, with an increase in vegetation

cover in the study region, the climate began to turn wetter and more favorable to the recovery and development of vegetation. The results described in this paper were also confirmed by the findings of Ma [37], Wang and Liu [38], and Wang et al. [39]. Ma conducted the study based on Chifeng Region Statistical Yearbook data combined with field surveys. The results of Ma's research show that the sandy land in the Chifeng Region is caused by a combination of long-term natural factors and human factors. Among them, the natural factors are mainly temperature, precipitation, and wind. Anthropogenic factors mainly include population pressure, cultivation, and grazing. After a long period of ecological management, as of 2006, the Chifeng Region achieved initial results in terms of improving the ecological environment and increasing the comprehensive productivity of the agricultural and animal husbandry industries. The results of Ma's study are basically consistent with the influence on Sandy land area in the Chifeng Region selected for the SEM of this study and can be mutually corroborated by the trend of sandy land area change in the Chifeng Region from 1990 to 2005 obtained by us, as discussed in Section 5.1. Through five consecutive years of field investigation and observation, Wang and Liu studied the plants applicable to the ecosystem restoration project in the Chifeng Region and proposed a management model and construction method for sandy land. Their results show that the Ecosystem restoration project in the Chifeng Region plays an important role in limiting the expansion of Sandy land and other aspects. This is consistent with the selection of the Ecosystem restoration project area as an important input element of the SEM in our study. Wang et al. utilize meteorological data, land use type data, and statistical data of cities in the Inner Mongolia Autonomous Region of China to evaluate the spatial and temporal evolution of ecological vulnerability in Inner Mongolia from three aspects: ecological, economic, and social. The results of Wang et al.'s study show that the ecological vulnerability of the eastern part of Inner Mongolia, where the Chifeng Region is located, is in a state of gradual decline. This finding is basically consistent with the trend of the area change in sandy land in the Chifeng Region and the factors affecting the change in the sandy land area derived from our study.

Table 5. Combined path coefficients for each driving factor.

Driving Factor	Arable Land Area	Population Size	Livestock Volume	Precipitation	Evaporation	Number of Sandy Wind Days	Ecosystem Restoration Project Area
Integrated path coefficient	0.129	0.119	0.153	−0.054	0.24	0.16	−0.26

5.3. Limitations and Future Research

In this study, CNN extraction with fused dynamic convolution was performed for sandy land areas using Landsat 4–5 TM, Landsat 7 ETM+, and Landsat 8 OLI multi-year multispectral ground observations. However, the method used in this study has some limitations. To begin with, this approach is dependent on the availability of a significant amount of sample data and a well-balanced sample distribution. Despite the huge sample size in this study, the intra-class variability of the samples was modest, and the sandy land targets were not visible enough in the sample images. This may have had an impact on the model's accuracy. Secondly, the sample data were images captured using various sensors, which could have affected the estimation accuracy. Furthermore, imaging variables such as weather and image resolution could also have had an impact on the findings.

This technology will be tested for other forms of feature extraction similar to sandy land in the future, such as desert and Gobi land. Furthermore, it will be worthwhile investigating the amount to which vegetation, water, and other factors impact the accuracy of sandy land extraction as the seasons change. Testing and analysis of multispectral data

from additional remote sensing image sources (e.g., Sentinel-2, GF-1) from other locations will also be conducted in our future research.

6. Conclusions

In this paper, we proposed a dynamic CNN model (DU-Net) by fusing dynamic convolution and U-Net to achieve large-range, long time series, and high-precision sandy land extraction based on Landsat images, in view of the characteristics of sandy land, i.e., the lack of obvious texture, the irregular shape, and the uneven demarcation in remote sensing images. The proposed model achieved a sandy land extraction accuracy of 86.32% in IoU, 93.22% in precision, 94.5% in recall, and 92.66% in F_1-score. Compared with the original U-Net model, the IoU, precision, recall, and F_1-score were improved by 4.68%, 2.33%, 3.09%, and 2.76%, respectively. On this premise, we acquired the geographical and temporal evolution trends of sandy land in the Chifeng region from 1990 to 2020 using structural equation modeling and driving force analysis. The data demonstrated that the sandy land area in the Chifeng region increased and subsequently decreased over the research period, with the sandy land area peaking around the year 2000. Furthermore, human socioeconomic activities have been the primary driving factor for the changes in sandy land area in the Chifeng region. The adoption of sand control policies and ecosystem restoration initiatives in the research region has resulted in an increase in the amount of forestable land while decreasing the number of sandy wind days, which has slowed down the spread of sandy land even more. The climate has also become wetter, which has aided in the development and recuperation of flora. As a result, the weather circumstances have served as additional driving factors. The spatial resolution of the long time series Landsat images chosen for this work is low, which may have resulted in some extraction mistakes, and the extraction accuracy could be further enhanced with the use of high-resolution images. In comparison to earlier research on the extraction of sandy land areas using long time series multispectral remote sensing data, this work represents a potentially useful strategy and a novel viewpoint on the correct extraction of varied targets in remote sensing imagery.

Author Contributions: Conceptualization, H.Z. and B.Z.; methodology, H.Z., B.Z., X.C. and J.L.; software, H.Z.; validation, H.Z.; writing—original draft preparation, B.Z.; writing—review and editing, H.Z., B.Z. and X.C.; visualization, H.Z.; project administration, H.Z. and B.Z.; funding acquisition, W.S. and J.D. All authors have read and agreed to the published version of the manuscript.

Funding: This work was supported in part by the National Natural Science Foundation of China under Grants 42071343, 42071428, 42204031. and Project funded by China Postdoctoral Science Foundation: 2022MD723791.

Institutional Review Board Statement: Not applicable.

Informed Consent Statement: Not applicable.

Data Availability Statement: Not applicable.

Acknowledgments: We are very grateful to all the reviewers, institutions, and authors for their help and advice on our work.

Conflicts of Interest: All authors declare that they have no conflict of interest.

References

1. Neely, C.; Bunning, S. Review of evidence on drylands pastoral systems and climate change. *Land Water Discuss. Pap.* **2009**, *6*, 103.
2. PNUMA. *Status of Desertification and Implementation of the United Nations Plan of Action to Combat Desertification: Report of the Executive Director*; United Nations Environment Programme: Nairobi, Kenya, 1991.
3. Wang, T.; Yan, C.Z.; Song, X.; Xie, J.L. Monitoring recent trends in the area of aeolian desertified land using Landsat images in China's Xinjiang region. *ISPRS J. Photogramm. Remote Sens.* **2012**, *68*, 184–190.
4. Wang, H.; Ma, M.; Geng, L. Monitoring the recent trend of aeolian desertification using Landsat TM and Landsat 8 imagery on the north-east Qinghai-Tibet Plateau in the Qinghai Lake basin. *Nat. Hazards* **2015**, *79*, 1753–1772. [CrossRef]

5. Zhang, F.; Tiyip, T.; Feng, Z.D.; Kung, H.T.; Johnson, V.C.; Ding, J.L.; Tashpolat, N.; Sawut, M.; Gui, D.W. Spatio-Temporal Patterns of Land Use/Cover Changes Over the Past 20 Years in the Middle Reaches of the Tarim River, Xinjiang, China. *Land Degrad. Dev.* **2015**, *26*, 284–299. [CrossRef]
6. Poulos, H.M. Mapping fuels in the Chihuahuan Desert borderlands using remote sensing, geographic information systems, and biophysical modeling. *Can. J. For. Res.* **2009**, *39*, 1917–1927. [CrossRef]
7. Feng, Y.M.; Wu, B.; Zhou, N.; Che, T.T.; Wang, F.; Cong, R.C.; Cao, Y.L.; Lu, Q. Gobi Classification System Based on Remote Sensing Image Recognition. *J. Desert Res.* **2013**, *33*, 635–641.
8. Varma, G.S.; Shah, V.; Buddhiraju, K.M. Segmentation of desert sand dunes. *Remote Sens. Lett.* **2014**, *5*, 961–970.
9. Schlesinger, W.H.; Reynolds, J.F.; Cunningham, G.L.; Huenneke, L.F.; Jarrell, W.M.; Virginia, R.A.; Whitford, W.G. Biological feedbacks in global desertification. *Science* **1990**, *247*, 1043–1048. [CrossRef]
10. Zongfan, B.; Ling, H.; Xuhai, J.; Ming, L.; Liangzhi, L.; Huiqun, L.; Jiaxin, L. Spatiotemporal evolution of desertification based on integrated remote sensing indices in Duolun County, Inner Mongolia. *Ecol. Inform.* **2022**, *70*, 101750. [CrossRef]
11. Wang, J.; Wang, J.; Yu, D.; Teng, D.; He, B.; Chen, X.; Ge, X.; Zhang, Z.; Wang, Y.; Yang, X.; et al. Machine learning-based detection of soil salinity in an arid desert region, Northwest China: A comparison between Landsat-8 OLI and Sentinel-2 MSI. *Sci. Total Environ.* **2020**, *707*, 136092. [CrossRef]
12. Li, J.; Zhao, L.; Xu, B.; Yang, X.; Jin, Y.; Gao, T.; Yu, H.; Zhao, F.; Ma, H.; Qin, Z. Spatiotemporal variations in grassland desertification based on Landsat images and spectral mixture analysis in Y anchi county of Ningxia, China. *IEEE J. Sel. Top. Appl. Earth Obs. Remote Sens.* **2014**, *7*, 4393–4402. [CrossRef]
13. Lecun, Y.; Boser, B.; Denker, J. Backpropagation Applied to Handwritten Zip Code Recognition. *Neural Comput.* **1989**, *1*, 541–551. [CrossRef]
14. Hugo, L. Exploring Strategies for Training Deep Neural Networks. *J. Mach. Learn. Res.* **2009**, *1*, 1–40.
15. Long, J.; Shelhamer, E.; Darrell, T. Fully convolutional networks for semantic segmentation. In Proceedings of the IEEE Conference on Computer Vision and Pattern Recognition, Boston, MA, USA, 12 June 2015; pp. 3431–3440.
16. Ronneberger, O.; Fischer, P.; Brox, T. *U-Net: Convolutional Networks for Biomedical Image Segmentation*; Springer International Publishing: Berlin/Heidelberg, Germany, 2015.
17. Zhou, K.; Zhang, Z.; Liu, L.; Miao, R.; Yang, Y.; Ren, T.; Yue, M. Research on SUnet Winter Wheat Identification Method Based on GF-2. *Remote Sens.* **2023**, *15*, 3094. [CrossRef]
18. Jiang, T.; Freudenberg, M.; Kleinn, C.; Ecker, A.; Nölke, N. The Impacts of Quality-Oriented Dataset Labeling on Tree Cover Segmentation Using U-Net: A Case Study in WorldView-3 Imagery. *Remote Sens.* **2023**, *15*, 1691. [CrossRef]
19. He, C.; Liu, Y.; Wang, D.; Liu, S.; Yu, L.; Ren, Y. Automatic Extraction of Bare Soil Land from High-Resolution Remote Sensing Images Based on Semantic Segmentation with Deep Learning. *Remote Sens.* **2023**, *15*, 1646. [CrossRef]
20. Cho, N.; Shin, H.S.; Tsourdos, A.; Amato, D. Incremental Correction in Dynamic Systems Modelled with Neural Networks for Constraint Satisfaction. *arXiv* **2022**, arXiv:2209.03698.
21. Othmani, M.; Ezzedine, Y.; Wang, Q.G. Event Detection in Clustered Wireless Sensor Networks Using Dynamic Cell Structures Neural Networks. *Adhoc Sens. Wirel. Netw.* **2022**, *51*, 141–171.
22. Jiang, Z.H.; Yu, W.; Zhou, D.; Chen, Y.; Feng, J.; Yan, S. ConvBERT: Improving BERT with Span-based Dynamic Convolution. *Adv. Neural Inf. Process. Syst.* **2020**, *33*, 12837–12848.
23. Feng, M.; Sun, X.; Dong, J.; Zhao, H. Gaussian Dynamic Convolution for Semantic Segmentation in Remote Sensing Images. *Remote Sens.* **2022**, *14*, 5736. [CrossRef]
24. Onojeghuo, A.O.; Miao, Y.; Blackburn, G.A. Deep ResU-Net Convolutional Neural Networks Segmentation for Smallholder Paddy Rice Mapping Using Sentinel 1 SAR and Sentinel 2 Optical Imagery. *Remote Sens.* **2023**, *15*, 1517. [CrossRef]
25. Zhang, L.; Li, Y. Occurrence and Nutrition Indicators of Alfalfa with Leptosphaerulina in Chifeng, Inner Mongolia. *Agriculture* **2022**, *12*, 1465. [CrossRef]
26. Wang, L.; Wang, X.; Wang, D.; Qi, B.; Zheng, S.; Liu, H.; Luo, C.; Li, H.; Meng, L.; Meng, X.; et al. Spatiotemporal Changes and Driving Factors of Cultivated Soil Organic Carbon in Northern China's Typical Agro-Pastoral Ecotone in the Last 30 Years. *Remote Sens.* **2021**, *13*, 3607. [CrossRef]
27. Xu, H. Evaluation of Two Absolute Radiometric Normalization Algorithms for Pre-processing of Landsat Imagery. *J. China Univ. Geosci.* **2006**, *2*, 146–150+157. [CrossRef]
28. Bodechtel, J.; Haydn, R.; Dibernardo, G.; Hiller, K.; Jaskolla, F.; Leisen, H.; Muenzer, U.; Nithack, J.; Smolka, A. *Application of LANDSAT Data and Digital Image Processing*; No. NASA-CR-158102; NASA: Washington, DC, USA, 1978.
29. Paisley, E.C.I.; Lancaster, N.; Gaddis, L.R.; Greeley, R. Discrimination of active and inactive sand from remote sensing: Kelso dunes, Mojave desert, California. *Remote Sens. Environ.* **1991**, *37*, 153–166. [CrossRef]
30. Muthén, B. A general structural equation model with dichotomous, ordered categorical, and continuous latent variable indicators. *Psychometrika* **1984**, *49*, 115–132. [CrossRef]
31. Lefcheck, J.S. piecewiseSEM: Piecewise structural equation modelling in r for ecology, evolution, and systematics. *Methods Ecol. Evol.* **2016**, *7*, 573–579. [CrossRef]
32. Mardani, A.; Streimikiene, D.; Zavadskas, E.K.; Cavallaro, F.; Nilashi, M.; Jusoh, A.; Zare, H. Application of Structural Equation Modeling (SEM) to Solve Environmental Sustainability Problems: A Comprehensive Review and Meta-Analysis. *Sustainability* **2017**, *9*, 1814. [CrossRef]

33. Song, W.; Zhang, Z.; Zhang, B.; Jia, G.; Zhu, H.; Zhang, J. ISTD-PDS7: A Benchmark Dataset for Multi-Type Pavement Distress Segmentation from CCD Images in Complex Scenarios. *Remote Sens.* **2023**, *15*, 1750. [CrossRef]
34. Zhang, G.P.; Liu, J.Y.; Zhang, Z.X.; Zhao, X.L.; Zhou, Q.B. Remote Sensing Based Analysis of the Distribution Pattern and Dynamic Changes of Sandy Land in China from 1995 to 2000. *Acta Ecol. Sin.* **2002**, *22*, 1500–1506+1574.
35. Zhang, L. Analysis of the suitability of agro-pastoral selection in the mixed agro-pastoral zone in northern China: The case of the Horqin sandy area. *Res. Soil Water Conserv.* **2007**, *14*, 46–50.
36. Zhu, H.; Zhang, B.; Song, W.; Dai, J.; Lan, X.; Chang, X. Power-Weighted Prediction of Photovoltaic Power Generation in the Context of Structural Equation Modeling. *Sustainability* **2023**, *15*, 10808. [CrossRef]
37. Ma, A. Sand management, greening and enrichment—Investigation report on the management of Horqin sand and Hunsandak sand in Chifeng city. *For. Econ.* **2006**, *7*, 11–14+21.
38. Wang, S.; Liu, Y. Study on Plant Sand Block Harness Model for Floating Sand of Chifeng City. *J. Soil Water Conserv.* **2005**, *4*, 144–147. [CrossRef]
39. Wang, Y.Q.; Song, S.Y.; Wang, J.; Li, H.F.; Xu, D.Y.; Li, L.T. Vulnerability evolution of the ecological-economic-social complex system and the key influencing factors in the sandy region of Inner Mongolia from 2000 to 2018. *Acta Ecol. Sin.* **2023**, *43*, 2271–2286.

Disclaimer/Publisher's Note: The statements, opinions and data contained in all publications are solely those of the individual author(s) and contributor(s) and not of MDPI and/or the editor(s). MDPI and/or the editor(s) disclaim responsibility for any injury to people or property resulting from any ideas, methods, instructions or products referred to in the content.